Emission of charged particles from excited compound nuclei

Sh. A. Kalandarov,[1,2] G. G. Adamian,[1,2,*] N. V. Antonenko,[1] and W. Scheid[3]

[1]*Bogoliubov Laboratory of Theoretical Physics, Joint Institute for Nuclear Research, Dubna, RU-141980 Moscow, Russia*

[2]*Institute of Nuclear Physics, Tashkent, UZ-702132 Tashkent, Uzbekistan*

[3]*Institut für Theoretische Physik der Justus-Liebig-Universität, D-35392 Giessen, Germany*

(Received 17 August 2010; published 4 October 2010)

The process of complex fragment emission is studied within the dinuclear system model. Cross sections of complex fragment emission are calculated and compared with experimental data for the reactions ^{3}He + ^{nat}Ag, ^{78,86}Kr + ^{12}C, and ^{63}Cu + ^{12}C. The mass distributions of the products of these reactions, isotopic distributions for the ^{3}He + ^{nat}Ag and ^{78}Kr + ^{12}C reactions, and average total kinetic energies of the products of the ^{78}Kr + ^{12}C reaction are predicted.

DOI: 10.1103/PhysRevC.82.044603 PACS number(s): 25.70.Gh, 24.10.Pa, 24.60.Dr

I. INTRODUCTION

Emission of complex or intermediate mass fragments ($Z > 2$) in low- and intermediate-energy nuclear reactions has been the subject of both experimental and theoretical interest for many years [1–4]. Early studies of this process [5–8] revealed that two components contributed to multiplicity: a fast, nonequilibrium component, producing light fragments at forward angles, and a relaxed component, producing fragments at all angles. Systematic studies of the relaxed component at low bombarding energies demonstrated the compound nucleus (CN) nature of the emission process [9,10]. The excitation functions for the equilibrium emission of complex fragments are reminiscent of fission excitation functions [11]. The dependence of the emission barriers on the mass asymmetry determines the charge and mass distributions of the emitted fragments [12]. Modulation of the potential energy along the mass-asymmetry coordinate is responsible for the strong variation of the cross sections with mass asymmetry. For a heavy CN, the mass distribution of decay products shows a peak at symmetry (fission peak) and two wings at extreme asymmetries (evaporation wings). For a light CN, the peak at symmetry disappears, to be replaced by a minimum in a U-shaped mass distribution [2].

There are different models for describing complex fragment emission. In the thermodynamical approach [13,14] the complex fragment emission width is obtained with the modified Weisskopf formula. This model disregards the distribution of excited energy between the emitted complex fragment and partner nucleus as well as the influence of the angular momentum on the emission. The latter simplification is justified only for complex nuclei (CNs) produced in reactions with p, d, and α particles. As will be seen, in CNs produced in heavy-ion reactions the angular momentum strongly influences the decay probabilities of complex fragments. The code GEMINI [15] treats the sequential statistical evaporation and binary decay of a hot CN and makes a sharp distinction between the decay widths for emission of light particles and the widths for emission of complex fragments. The widths for emission of light particles are calculated using the Hauser-Feshbach approach with sharp cutoff transmission coefficients. The complex fragment emission width is treated within the generalized transition-state concept proposed in Ref. [12]. The rotating finite-range model [16] or the rotating liquid-drop model is used to calculate the conditional barriers for binary division. As found, the mass asymmetric fission barriers extracted from the experimental excitation functions lie between the values calculated with these two models [17,18].

In the present paper, we consider complex fragment emission within the dinuclear system (DNS) model [19–22]. Cluster emission is treated under the assumption that light clusters are produced by collective motion of the nuclear system in the charge asymmetry coordinate, with further thermal escape over the Coulomb barrier. Emission barriers for complex fragments are calculated within the DNS model by using the double-folding procedure (with the Skyrme-type density-dependent effective nucleon-nucleon interaction) for the nuclear part of the nucleus-nucleus interaction potential. Both evaporation and binary decay are treated in the same way. The important role of the angular momentum of the CN in the binary decay process is demonstrated. Correct definition of the emission barriers and of their dependence on the angular momentum allows us to calculate the charge, mass, and kinetic energy distributions of the emitted complex fragments. For excitations treated, the temperature effect on emission barriers is not taken into consideration for the reactions of interest. The main ingredient in our description is the sophisticated potential energy as a function of the angular momentum. The model is described in Sec. II. Results of our calculations for the reactions ^{3}He + ^{nat}Ag, ^{78,86}Kr + ^{12}C, and ^{63}Cu + ^{12}C are presented in Sec. III. The conclusions are given in Sec. IV.

II. FORMATION AND DECAY OF THE COMPOUND NUCLEUS (CN) AND DINUCLEAR SYSTEM (DNS)

A. Model

The emission process of complex fragments from an excited nuclear system involves the motions in charge and mass asymmetry coordinates, which are defined here by the charge and mass (neutron) numbers $Z = Z_1$ and $A = A_1$ ($N = N_1 = A - Z$) of a light nucleus of the DNS [19–22] formed by two touching nuclei and the motion in the relative distance R between the centers of mass of the nuclei. In

*adamian@theor.jinr.ru

 ©2010 The American Physical Society

the decoupled approximation, binary decay consists of two steps: (i) clustering or the formation of an asymmetric DNS in the excited state with some probability and (ii) the decay of this DNS by the thermal overcoming the barrier in the nucleus-nucleus potential. The probability of cluster formation is calculated statistically using the stationary solution of the master equation with respect to the charge and mass asymmetries and depends on the potential energy of the DNS configurations at touching distance and thermodynamical temperature of the system. The probability of DNS decay in the R coordinate is calculated using the transition-state method. This decay process depends on the thermodynamical temperature of the DNS and the difference in the potential energies of the DNS configurations at the touching distance versus the barrier position.

The cross section of the charge-particle emission is calculated as follows:

$$\sigma_{Z,A}(E_{\text{c.m.}}) = \sum_{J=0}^{J_{\max}} \sigma_{Z,A}(E_{\text{c.m.}}, J) = \sum_{J=0}^{J_{\max}} \sigma_{\text{cap}}(E_{\text{c.m.}}, J) W_{Z,A}(E^*_{\text{CN}}, J), \quad (1)$$

where $\sigma_{\text{cap}}(E_{\text{c.m.}}, J)$ is the partial capture cross section and $W_{Z,A}(E^*_{\text{CN}}, J)$ is the emission probability of a given particle. The maximum value of angular momentum $J = J_{\max}$ is set as the minimum from the values of kinematical and critical angular momenta (see Sec. II C). Here we consider the decay of an excited CN as a sequential light-particle evaporation, which includes neutrons, protons, deuterons, tritons, and a cluster ($Z \geqslant 2$) emission.

CN formation and its consequent decay are not necessarily the ultimate results of the evolution of the initial DNS. In addition to contributions from a CN decay, the binary decay component is related to the quasifission (or multinucleon transfer) mechanism. In our model the fragments are produced as binary decay products of the DNS formed during the diffusion process along the mass (charge) asymmetry coordinate with and without stages of CN formation. The dominant reaction mechanism (complete fusion or quasifission) depends on the entrance channel and on the value of the angular momentum deposited into the system. For the reactions considered, the CN configuration seems to be energetically more favorable than any DNS configuration even at $J = J_{\max}$. Because of this fact, the quasifission component is small in comparison with the complete fusion component. In our model both components are taken into consideration.

B. DNS potential energy and nucleus-nucleus interaction potential

Assuming a small overlap of nuclei in the DNS, the potential energy (driving potential) of the DNS is calculated as follows [21,22]:

$$U(R, Z, A, J) = B_1 + B_2 + V(R, Z, A, \beta_1, \beta_2, J) - \left[B_{12} + E^{\text{rot}}_{12}(J)\right], \quad (2)$$

where B_1 and B_2 are the mass excesses of fragments in their ground states, and β_1 and β_2 are their quadrupole deformation parameters, which are taken from Ref. [23], for even-even nuclei. For the quadruple deformation parameter of an odd nucleus, we choose the maximal value from the deformation parameters of neighboring even-even nuclei. Experimental values of B_1 and B_2 are used, if available in Ref. [24]. Otherwise, we use values from Ref. [25]. The potential energy is normalized to the potential energy $B_{12} + E^{\text{rot}}_{12}(J)$ of the rotating CN. Here, B_{12} is the mass excess of the CN and the rotational energy E^{rot}_{12} of the CN is defined as $E^{\text{rot}}_{12}(J) = \hbar^2 J(J+1)/2\Im_{\text{CN}}$, where $\Im_{\text{CN}}$ is the rigid-body moment of inertia of the CN. The nucleus-nucleus potential,

$$V(R, Z, A, \beta_1, \beta_2, J) = V_C(R, Z, A, \beta_1, \beta_2) + V_N(R, Z, A, \beta_1, \beta_2) + \frac{\hbar^2 J(J+1)}{2\Im(R, A, \beta_1, \beta_2)}, \quad (3)$$

in Eq. (2) is the sum of the Coulomb potential V_C, the nuclear potential V_N, and the centrifugal potential (last summand). The moment of inertia $\Im$ of the DNS formed is calculated in the sticking limit as

$$\Im(R, A, \beta_1, \beta_2) = k_0(\Im_1 + \Im_2 + \mu R^2), \quad (4)$$

where the moments of inertia $\Im_i$ ($i = 1, 2$) of the DNS nuclei are obtained in the rigid-body approximation:

$$\Im_i = \frac{1}{5} m_0 A_i (a_i^2 + b_i^2),$$
$$a_i = R_{0i}\left(1 - \frac{\beta_i^2}{4\pi}\right)\left(1 + \sqrt{\frac{5}{4\pi}}\beta_i\right), \quad (5)$$
$$b_i = R_{0i}\left(1 - \frac{\beta_i^2}{4\pi}\right)\left(1 - \sqrt{\frac{5}{16\pi}}\beta_i\right).$$

As known from the experimental study, the moments of inertia of strongly deformed nuclear states are very close to 85% of those in the rigid-body limit [26]. We also set $k_0 = 0.85$ in our calculations. When the nucleus-nucleus potential is calculated in the entrance channel (the capture stage), in Eq. (3) the value of $\Im(R, A, \beta_1, \beta_2)$ is replaced by $\Im = \mu R^2$.

For the nuclear part of the nucleus-nucleus potential, we use the double-folding formalism [21]

$$V_N = \int \rho_1(\mathbf{r_1})\rho_2(\mathbf{R} - \mathbf{r_2}) F(\mathbf{r_1} - \mathbf{r_2})\, d\mathbf{r_1} d\mathbf{r_2}, \quad (6)$$

where $F(\mathbf{r_1} - \mathbf{r_2}) = C_0[F_{\text{in}}\frac{\rho_0(\mathbf{r_1})}{\rho_{00}} + F_{\text{ex}}(1 - \frac{\rho_0(\mathbf{r_1})}{\rho_{00}})]\delta(\mathbf{r_1} - \mathbf{r_2})$ is the Skyrme-type density-dependent effective nucleon-nucleon interaction, which is known from the theory of finite Fermi systems [27], and $\rho_0(\mathbf{r}) = \rho_1(\mathbf{r}) + \rho_2(\mathbf{R} - \mathbf{r})$, $F_{\text{in,ex}} = f_{\text{in,ex}} + f'_{\text{in,ex}}\frac{(N-Z)(N_2-Z_2)}{(N+Z)(N_2+Z_2)}$. Here, $\rho_1(\mathbf{r_1})$ and $\rho_2(\mathbf{r_2})$ are the nucleon densities of the light and heavy nuclei of the DNS, respectively, and N_2 (Z_2) is the neutron (charge) number of the heavy nucleus of the DNS. Our calculations are performed with the following set of parameters: $C_0 =$ 300 MeV fm^3, $f_{\text{in}} = 0.09$, $f_{\text{ex}} = -2.59$, $f'_{\text{in}} = 0.42$, $f'_{\text{ex}} = 0.54$, and $\rho_{00} = 0.17$ fm^{-3} [27]. The densities of the nuclei are

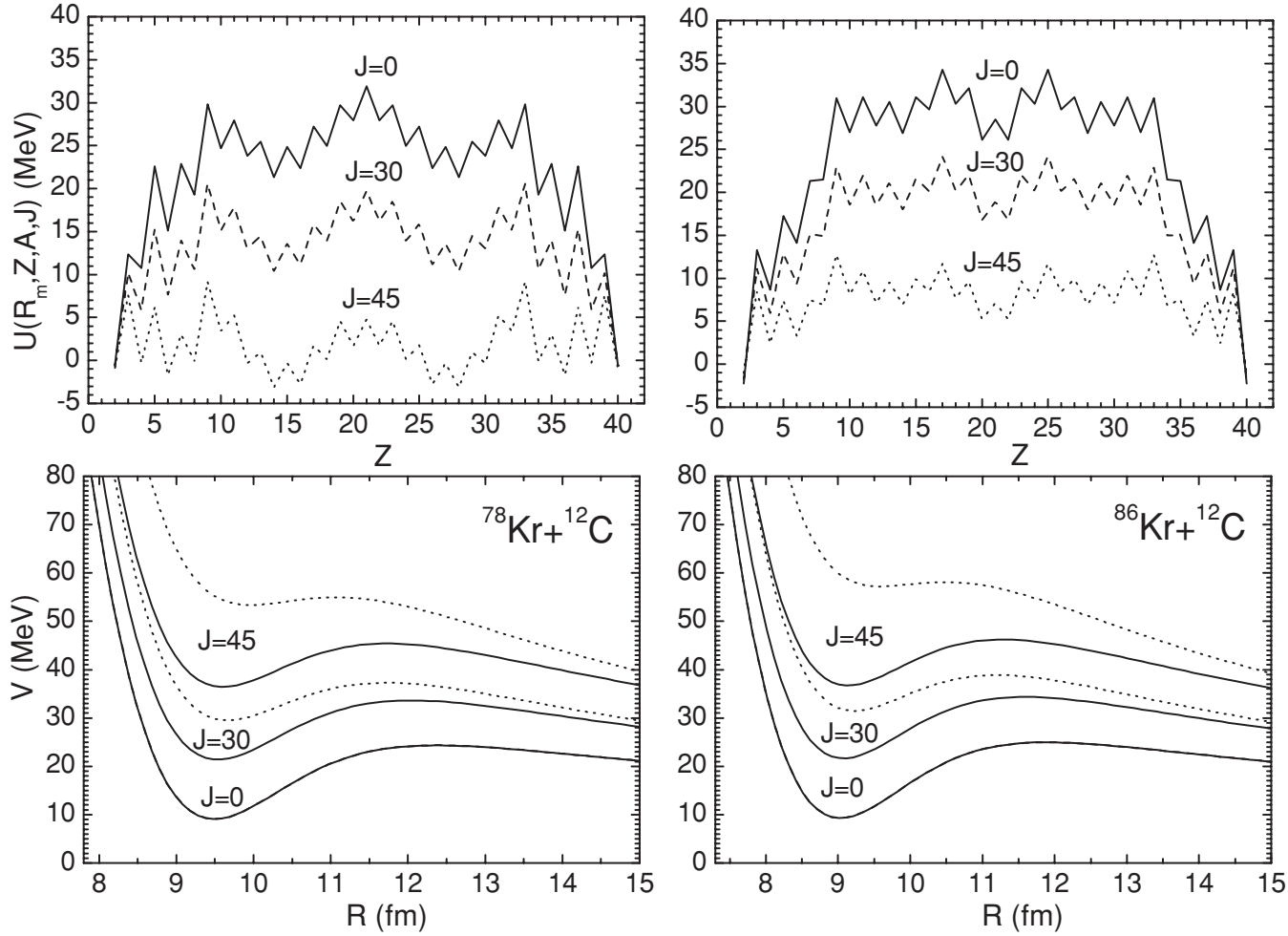

FIG. 1. (Right) Dependencies of the nucleus-nucleus potential V on R (lower), in the entrance (dotted lines) and the exit (solid lines) channels, and of the potential energies $U(R_m, Z, A, J)$ of the DNS at $R = R_m$ on the charge number Z of one of the DNS nuclei (upper) for the ^{86}Kr + ^{12}C reaction. The value of A relates to Z to supply the minimum of U. Results calculated for the angular momenta $J = 0, 30, 45$ are presented. The value of U is normalized to the energy of the rotating compound nucleus. (Left) The same as the right side, but for the ^{78}Kr + ^{12}C reaction.

taken in the two-parameter symmetrized Woods-Saxon form with the nuclear radius parameter $r_0 = 1.02$–1.16 fm and the diffuseness parameter $a = 0.51$–0.56 fm, depending on the charge and mass numbers of the nucleus [21].

With the density-dependent effective nucleon-nucleon interaction a repulsive core appears in V (see the lower plots in Fig. 1), which prevents the motion to smaller distances, $R < R_1[1 + \sqrt{5/(4\pi)}\beta_1] + R_2[1 + \sqrt{5/(4\pi)}\beta_2]$, and reflects the action of the Pauli principle. Owing to the sum of the repulsive Coulomb and centrifugal summands with the attractive nuclear one in Eq. (3), the nucleus-nucleus potential has a pocket with a minimum situated for pole-pole orientation at the touching distance between the nuclei $R = R_m \approx R_1[1 + \sqrt{5/(4\pi)}\beta_1] + R_2[1 + \sqrt{5/(4\pi)}\beta_2] + 0.5$ fm, where $R_i = r_0 A_i^{1/3}$ are the radii of interacting nuclei. The DNS is localized in the minimum of this pocket (Fig. 1). At $J = 0$, the position of the Coulomb barrier in V corresponds to $R = R_b \approx R_m + 2$ fm in the DNS under consideration. Then the depth of the potential pocket is $B_R^{\rm qf}(Z, A, J) = V(R_b, Z, A, \beta_1, \beta_2, J) - V(R_m, Z, A, \beta_1, \beta_2, J)$. The barrier $B_R^{\rm qf}$, called the quasifission barrier, prevents the DNS decay in R. The depth $B_R^{\rm qf}$ of the potential pocket decreases with increasing J because of the growth of the repulsive centrifugal part in Eq. (3). In the entrance channel the potential pocket disappears at some critical value $J = J_{\rm cr}$ (see dashed lines in Fig. 1). So capture of the projectile by the target is impossible at angular momenta larger than $J_{\rm cr}$. The depth of the potential pocket depends also on the charge asymmetry of the DNS corresponding to a given CN. For an asymmetric DNS, the interaction potential pocket is deeper than that for a more symmetric configuration.

The potential energies $U(R_m, Z, A, J)$ of the DNS versus Z are presented in Fig. 1 at different values of J for the reactions ^{78,86}Kr + ^{12}C. Note that because the isotopic composition of the nuclei forming the DNS is chosen with the condition of an N/Z equilibrium in the system [19], the mass and charge evolutions are related to each other. Because the mode responsible for the N/Z equilibrium in the DNS is the fast

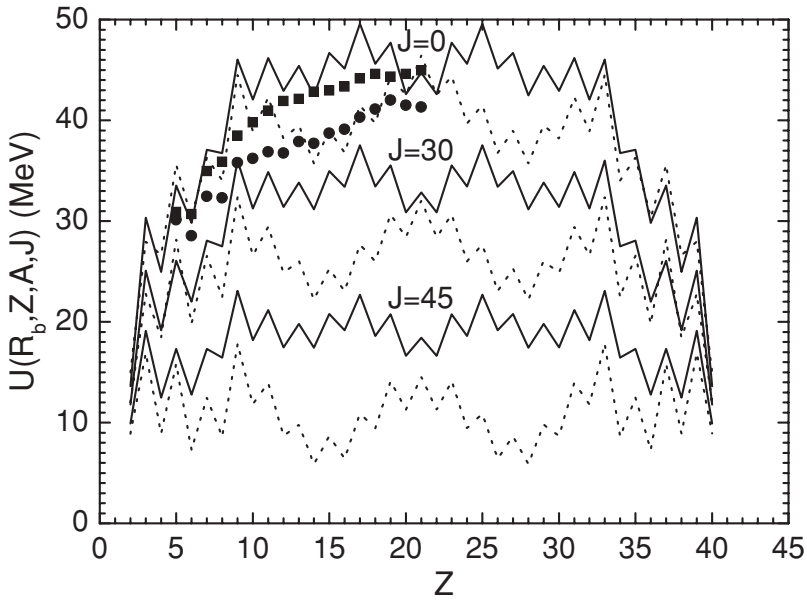

FIG. 2. Potential energies $U(R_b, Z, A, J)$ of the DNS at position $R = R_b$ of the Coulomb barrier of V versus charge asymmetry (expressed by the Z value of one of the fragments) are presented at different values of angular momentum J for the reactions ^{78}Kr + ^{12}C (dashed line) and ^{86}Kr + ^{12}C (solid line). The value of A relates to Z to supply the minimum of U. The value of U is normalized to the energy of the rotating compound nucleus. Mass-asymmetric macroscopic fission barriers extracted from the experimental cluster decay cross sections in Ref. [17] are shown for the reactions ^{78}Kr + ^{12}C (filled circles) and ^{86}Kr + ^{12}C (filled squares).

one, the potential energies U are minimized with respect to the mass asymmetry for each fixed charge asymmetry. For the shown U with $J \leqslant J_{\max}$, the CN configuration seems to be energetically more favorable than any DNS configuration. Thus, the quasifission component is small in comparison with the complete fusion component. At high angular momenta, about $J \geqslant 60$, the potential energy U of a DNS, normalized to the energy of a rotating CN, is negative. This indicates that the complete fusion becomes energetically denied.

Note that the driving potential is sensitive to the total mass number of the DNS. Comparing the driving potentials for the reactions ^{78}Kr + ^{12}C and ^{86}Kr + ^{12}C (Fig. 1), one can conclude that the odd-even staggering decreases with increasing N/Z ratio in the system and the potential energy is flatter for a neutron-rich DNS. Figure 2 shows a comparison of the binary decay barriers obtained in our model for ^{90,98}Mo with the mass-asymmetric macroscopic fission barriers extracted from the experimental cluster decay cross sections in Ref. [17]; this is convincing evidence of the correctness of our potential energy calculations.

C. Capture cross section

The partial capture cross section is given as

$$\sigma_c(E_{\text{c.m.}}, J) = \pi \lambda\!\!\!^{-2}(2J+1)P_{\text{cap}}(E_{\text{c.m.}}, J), \tag{7}$$

where $\lambda\!\!\!^{-2} = \hbar^2/(2\mu E_{\text{c.m.}})$ is the reduced de Broglie wavelength and μ the reduced mass. The value of $\sigma_c(E_{\text{c.m.}}, J)$ defines the transition of the colliding nuclei over the Coulomb barrier with the probability $P_{\text{cap}}(E_{\text{c.m.}}, J)$ and the formation of the initial DNS when the kinetic energy $E_{\text{c.m.}}$ and angular momentum J of the relative motion are transformed into the excitation energy and angular momentum of the DNS. The transition probability is calculated with the Hill-Wheeler formula $P_{\text{cap}}(E_{\text{c.m.}}, J) = (1+\exp\{2\pi[V(R_b, Z_i, A_i, \beta_1 = 0, \beta_2 = 0, J) - E_{\text{c.m.}}]/\hbar\omega(J)\})^{-1}$, where the effective nucleus-nucleus potential V is approximated near the Coulomb barrier at $R = R_b$ by the inverted harmonic-oscillator potential with the barrier height $V(R_b, J)$ and the frequency $\omega(J)$.

The total capture cross section is

$$\sigma_c(E_{\text{c.m.}}) = \sum_{J=0}^{J_{\max}} \sigma_c(E_{\text{c.m.}}, J) = \pi \lambda\!\!\!^{-2} \sum_{J=0}^{J_{\max}} (2J+1)P_{\text{cap}}(E_{\text{c.m.}}, J), \tag{8}$$

where the maximum value of angular momentum $J_{\max}$ is limited by either the kinematical angular momentum $J_{\text{kin}} = \{2\mu[E_{\text{c.m.}} - V(R_b, Z_i, A_i, \beta_1 = 0, \beta_2 = 0, J = 0)]\}^{1/2} R_b/\hbar$ or by the critical angular momentum J_{cr}, depending on which one is smaller: $J_{\max} = \min\{J_{\text{kin}}, J_{\text{cr}}\}$.

The excitation energy of the CN formed is determined as

$$E^*_{\text{CN}}(J) = E_{\text{c.m.}} + Q - E^{\text{rot}}_{12}(J), \tag{9}$$

where the Q value is determined as $Q = B_1 + B_2 - B_{12}$ and the rotational energy E^{rot}_{12} is not available for internal excitation. Because the potential energy of the DNS is determined relative to the CN potential energy, the local excitation energy of each DNS is

$$E^*_{Z,A}(J) = E^*_{\text{CN}}(J) - U(R_m, Z, A, J). \tag{10}$$

Then the temperatures of the CN and the DNS are $T_{\text{CN}}(J) = \sqrt{E^*_{\text{CN}}(J)/a}$ and $T_{Z,A}(J) = \sqrt{E^*_{Z,A}(J)/a}$, respectively, within the Fermi-gas model. The level density parameter a is taken as $a = 0.114A + 0.162A^{2/3}$ from Ref. [28].

D. Evolution of charge and mass asymmetries

The time evolution of the charge and mass asymmetry coordinates of a nuclear system is usually described in the framework of the transport model. In this approach the time dependence of the probability $P_{Z,A}(t)$ of finding a system at moment t in a state with charge Z and mass A asymmetries is

calculated by the master equation [29]

$$\frac{d}{dt}P_{Z,A}(t) = \Delta^{(-,0)}_{Z+1,A+1}P_{Z+1,A+1}(t) + \Delta^{(+,0)}_{Z-1,A-1}P_{Z-1,A-1}(t) + \Delta^{(0,-)}_{Z,A+1}P_{Z,A+1}(t) + \Delta^{(0,+)}_{Z,A-1}P_{Z,A-1}(t) - \left[\Delta^{(-,0)}_{Z,A} + \Delta^{(+,0)}_{Z,A} + \Delta^{(0,-)}_{Z,A} + \Delta^{(0,+)}_{Z,A}\right]P_{Z,A}(t), \tag{11}$$

with initial condition $P_{Z,A}(0) = \delta_{Z,Z_i}\delta_{A,A_i}$ (Z_i and A_i characterize the initial DNS). Here, the CN is treated as one of the available asymmetries. The transport coefficients [$\Delta^{(+,0)}_{Z,A}$, $\Delta^{(0,+)}_{Z,A}$] characterize the proton and neutron transfer rates from a heavy to a light nucleus or in the opposite direction [$\Delta^{(-,0)}_{Z,A}$, $\Delta^{(0,-)}_{Z,A}$]. In Eq. (11) we take only the transitions $Z \rightleftharpoons Z \pm 1$ and $N \rightleftharpoons N \pm 1$ into account, in the spirit of the independent-particle model. The time independence of the transport coefficients and the structure of Eq. (11) guarantee the existence of a stationary solution $P_{Z,A}(t \to \infty) = P_{Z,A}(E^*_{\rm CN}, J)$ of the master equation.

The lifetime of an excited CN (DNS) is predetermined by the time of neutron emission (the time of quasifission), which is sufficiently long to reach the mass and charge equilibrium limit in Eq. (11). Thus, in the treatment of the formation of complex fragments the equilibrium limit of the master equation can be imposed so that the probability $P_{Z,A}(E^*_{\rm CN}, J)$ is proportional to the relevant level density ρ. At a fixed total energy of the CN the level density is proportional to $\exp[-U(R_m, Z, A, J)/T_{\max}(J)]$, $T_{\max}(J) = \max[T_{\rm CN}(J), T_{Z,A}(J)]$ [29], and thus, the DNS formation probability is written in the following way:

$$P_{Z,A}(E^*_{\rm CN}, J) = \frac{\exp[-U(R_m, Z, A, J)/T_{\max}(J)]}{1 + \sum_{Z'=2,A'}\exp[-U(R_m, Z', A', J)/T_{\max}(J)]}. \tag{12}$$

According to Eq. (12), the potential energy $U(R_m, Z, A, J)$ completely determines the evolution of the excited system. For the reactions under consideration, $T_{\max}(J) = T_{\rm CN}(J)$.

The probability of thermal penetration of the Coulomb barrier (decay of the DNS in R into two fragments or binary decay with $Z \geqslant 2$) from the DNS represented by two nuclei trapped in a potential pocket can be written, in complete analogy with the fission probability in the transition-state formalism (at the high-temperature limit), as

$$P^R_{Z,A} \sim \exp\left[-B^{\rm qf}_R(Z, A, J)/T_{Z,A}(J)\right]. \tag{13}$$

From the experimental data [2] on complex fragment emission at low energies, one would conclude that fission and evaporation are the two obvious extremes of a single statistical decay process. The connection between them is provided in a very natural way by the mass asymmetry coordinate. Because of this, theoretical descriptions of the binary decay and the light-particle evaporation processes should be on the same basis, and we use the same expression, Eq. (13), to calculate the probabilities of neutron, proton, deuteron, and triton emissions. So, the competition between the evaporation channel and the binary decay channel is taken into consideration in a unique way. In the calculations the temperature and emission barriers for these particles are as follows: $T_{Z=0,A=0}(J) = T_{Z=0,A=1}(J) = T_{Z=1,A=0}(J) = T_{Z=1,A=1}(J) = T_{Z=1,A=1}(J) = T_{\rm CN}(J)$ and $B^{\rm qf}_R(Z = 0, A = 1, J) = B_n$ for a neutron with binding energy B_n, $B^{\rm qf}_R(Z = 1, A = 0, J) = B_p + V^{(p)}_C$ for a proton with binding energy B_p and Coulomb barrier $V^{(p)}_C$, $B^{\rm qf}_R(Z = 1, A = 1, J) = B_d + V^{(d)}_C$ for a deuteron with binding energy B_d and Coulomb barrier $V^{(d)}_C$, and $B^{\rm qf}_R(Z = 1, A = 2, J) = B_t + V^{(t)}_C$ for a triton with binding energy B_t and Coulomb barrier $V^{(t)}_C$. Coulomb barriers for the outgoing proton, deuteron, and triton are taken as in Ref. [20]:

$$V^{(i)}_C = \frac{e^2(Z' - 1)}{1.7\left[(A' - m_i)^{1/3} + m_i^{1/3}\right]}, \tag{14}$$

where Z' and A' are the charge and mass numbers of a nucleus that emits a light charge particle i ($i = p, d, t$) and m_i is the mass number of the light charge particle.

Binary cluster emission is imagined as a two-step process. The system evolves in charge and mass asymmetry coordinates to reach a statistical equilibrium in mass asymmetry coordinate so that the probability of finding the system in each DNS configuration and CN configuration depends on the potential energy $U(R_m, Z, A, J)$. After formation, the excited DNS can decay in R coordinate into two clusters if the local excitation energy of the DNS is high enough to overcome the barrier in R. So, the emission probability $W_{Z,A}(E^*_{\rm CN}, J)$ of a certain cluster is the product of the DNS formation probability and the DNS decay probability:

$$W_{Z,A}(E^*_{\rm CN}, J) = \frac{P_{Z,A}P^R_{Z,A}}{\sum_{Z',A'}P_{Z',A'}P^R_{Z',A'}} = \frac{\exp[-U(R_m, Z, A, J)/T_{\rm CN}(J)]\exp\left[-B^{\rm qf}_R(Z, A, J)/T_{Z,A}(J)\right]}{\sum_{Z',A'}\exp[-U(R_m, Z', A', J)/T_{\rm CN}(J)]\exp\left[-B^{\rm qf}_R(Z', A', J)/T_{Z',A'}(J)\right]}, \tag{15}$$

where the indexes Z' and A' go over all possible channels of disintegration, from neutron evaporation to symmetric splitting. Here, $U(R_m, Z, A, J) = 0$ for the n, p, d, and t evaporation channels. Thus, the competition between the evaporation channel and the binary decay channel is taken into consideration in a very natural way. We should stress that this competition depends strongly on the angular momentum of the system. With increasing angular momentum J, the CN has less excitation energy available for the evaporation of light particles, but at the same time the binary decay barrier $B^{\rm qf}_R$ decreases. The probability $W_{Z,A}$ increases with J more rapidly for a symmetric DNS than for asymmetric ones. Thus, the yields of fissionlike products grow with increasing angular momentum.

For the binary decay channel, the excitation energies of the emitted complex fragment and residue nucleus are, respectively,

$$E^*_L(Z,A,J) = \left[E^*_{Z,A}(J) - B^{\rm qf}_R(Z,A,J)\right]\frac{A}{A_t},$$
$$E^*_H(Z,A,J) = \left[E^*_{Z,A}(J) - B^{\rm qf}_R(Z,A,J)\right]\frac{A_2}{A_t}, \quad (16)$$

where $A_t = A + A_2$ is the total mass number of the DNS and $E^*_{Z,A}(J) - B^{\rm qf}_R(Z,A,J)$ the excitation energy of the DNS at the Coulomb barrier. We assume that the excitation energy and the angular momentum of the DNS are shared between the DNS nuclei proportionally to their mass numbers and moments of inertia, respectively.

III. CALCULATED RESULTS

In the calculations, we use formulas (1) and (15) to treat the sequential statistical decay (evaporation of light particles and/or binary decay) of a hot CN. The generation of a whole cascade of decay channels is performed by the Monte Carlo method. We continue to trace the decay processes until all fragments become cold (the excitation energy of fragments is lower than its neutron emission threshold). The number n of generations of events in the Monte Carlo technique was chosen according to the lowest decay probability, which is $\sim 1/n$. The number $n > 10^4$ of iterations is large enough to obtain calculated results with a high accuracy.

To test our method, we treated the charge distributions of emitted clusters for the reactions ^{3}He + $^{\rm nat}$Ag at $E_{\rm lab} =$ 30 MeV/nucleon ($J_{\rm max} = J_{\rm cr} = 15$ and $J_{\rm kin} = 17$) and ^{63}Cu + ^{12}C at $E_{\rm lab} = 12.6$ MeV/nucleon ($J_{\rm max} = J_{\rm cr} = 40$ and $J_{\rm kin} = 48$), leading to the CNs ^{111}In [$E^*_{\rm CN}(J=0) = 103.3$ MeV] and ^{75}Br [$E^*_{\rm CN}(J=0) = 130.6$ MeV], respectively. In Figs. 3 and 4 the calculated emission cross sections,

$$\sigma_Z(E_{\rm c.m.}) = \sum_A \sigma_{Z,A}(E_{\rm c.m.}), \quad (17)$$

are in good agreement with the experimental data [8,30]. The experimental maxima of the charge distributions are correctly reproduced. Odd-even effects (emission of even-Z fragments is preferred over that of fragments with odd Z values) are visible in the charge distributions for light fragments. This fact indicates the influence of the shell structure of the DNS nuclei on the evolution and decay of the system. Because the pairing energy of the DNS light nucleus decreases with increasing mass number A, odd-even effects become weaker for larger values of Z.

As already shown, the suggested method is suitable for predicting the charge yields. In Fig. 3 (lower) the mass distribution,

$$\sigma_A(E_{\rm c.m.}) = \sum_Z \sigma_{Z,A}(E_{\rm c.m.}), \quad (18)$$

of the products of the ^{3}He ($E_{\rm lab} = 30$ MeV/nucleon) + $^{\rm nat}$Ag reaction is predicted. The peaks in the light mass region correspond to the even-even nuclei ^{8}Be, ^{12}C, and ^{16}O. The reason is that the driving potential U has deep minima for corresponding DNSs. The isotopic distributions of the light

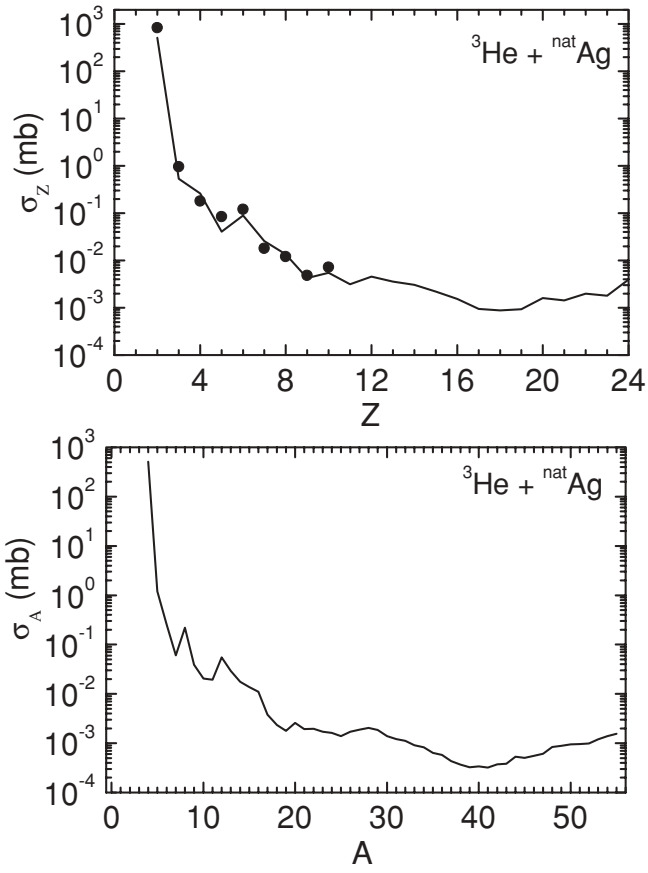

FIG. 3. Calculated charge (upper) and mass (lower) distributions for the ^{3}He + $^{\rm nat}$Ag reaction at bombarding energy $E_{\rm lab} =$ 30 MeV/nucleon. Experimental data (filled points) are taken from Ref. [8].

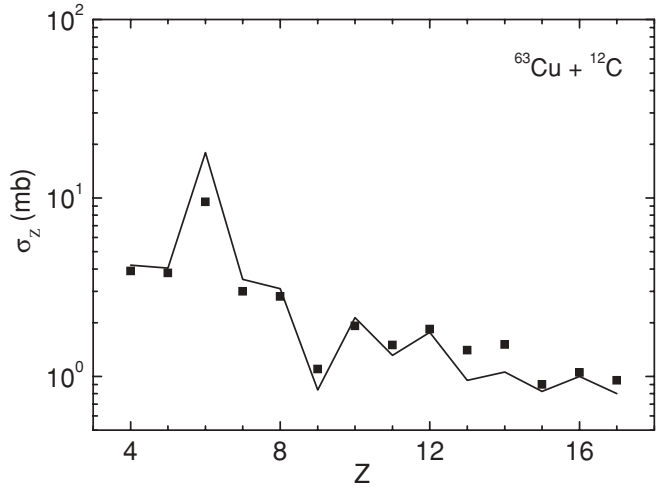

FIG. 4. Calculated charge distributions for the ^{63}Cu + ^{12}C reaction at bombarding energy $E_{\rm lab} = 12.6$ MeV/nucleon. Experimental data (filled points) are taken from Ref. [30].

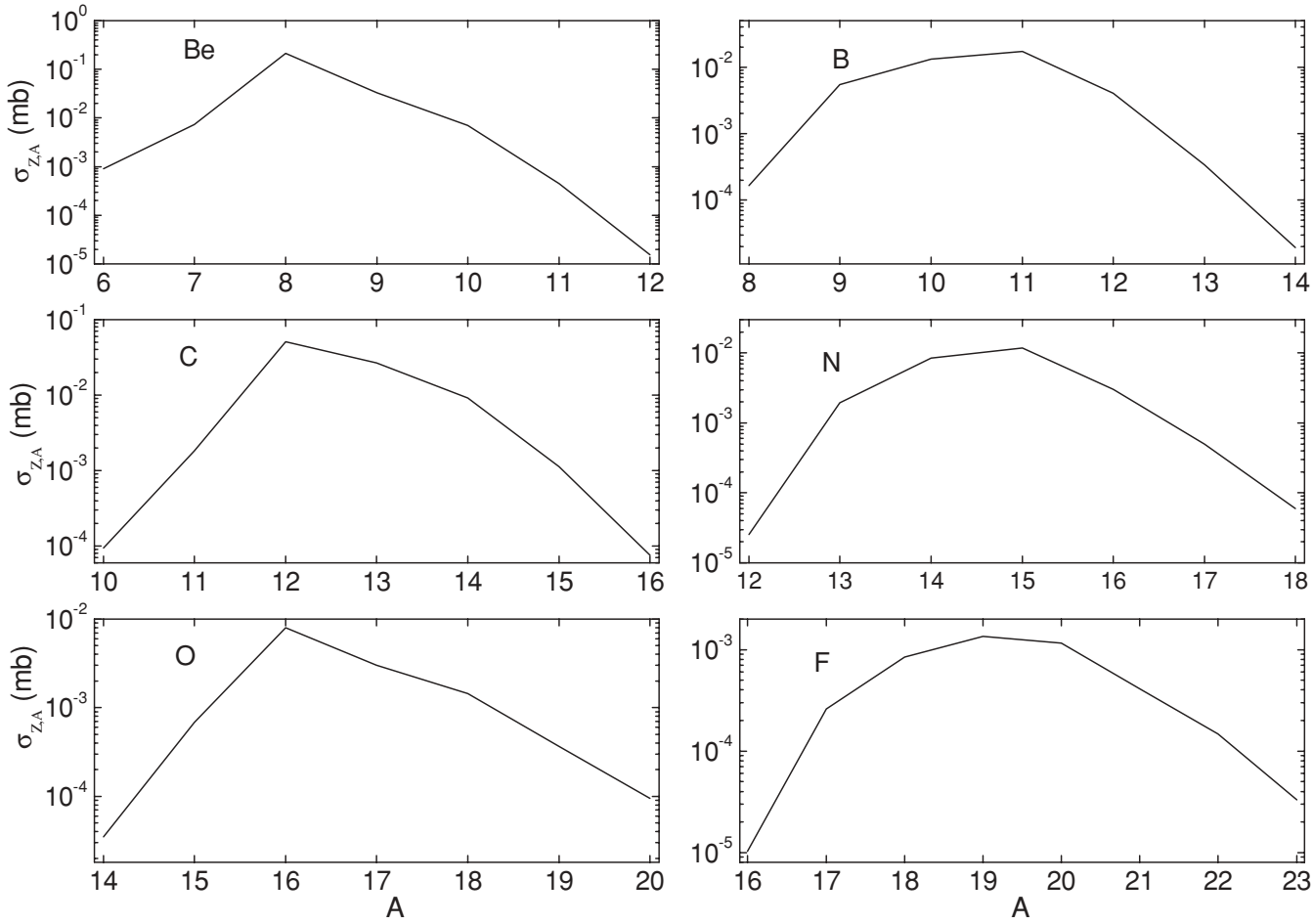

FIG. 5. Calculated isotopic distributions of binary decay products for the ^{3}He + ^{nat}Ag reaction at bombarding energy E_{lab} = 30 MeV/nucleon.

products emitted are predicted in Fig. 5, where one can see that the distributions for odd-Z nuclei are broader than those for neighboring even-Z nuclei. These predictions can be experimentally verified.

For the ^{78}Kr + ^{12}C reaction leading to the CN ^{90}Mo, the calculations of charge and mass distributions are performed at two different bombarding energies, E_{lab} = 8.52 and 11.37 MeV/nucleon (Fig. 6). The maximum angular momentum $J_{max} = J_{cr} = 42$ is determined by the critical angular momentum for both cases. For example, the Bass model [31] gives J_{max} = 43 and 47 at E_{lab} = 8.52 and 11.37 MeV/nucleon, respectively [17]. The agreement between the calculated and the experimental [17] Z distributions is quite good for both energies. Odd-even effects are again visible in the charge distributions for light fragments, while the excitation energies of the CN are quite high, $E^{*}_{CN}(J = 0)$ = 94.6 and 124.2 MeV for the given incident energies. The strong increase in the absolute cross sections with increasing bombarding energy is seen in Fig. 6. The high excitation energy of the CN leads to the high probability of binary decay. For example, the experimental yield for the carbon is 3.7 times larger at E_{lab} = 11.37 MeV/nucleon than at E_{lab} = 8.52 MeV/nucleon. The theoretical estimation gives a 3.45× difference.

The dependencies of the partial cross section

$$\sigma_Z(E_{c.m.}, J) = \sum_A \sigma_{Z,A}(E_{c.m.}, J) \tag{19}$$

on the angular momentum J for the carbon and calcium fragments are presented in Fig. 7 for the ^{78}Kr + ^{12}C reaction at the bombarding energy E_{lab} = 8.52 MeV/nucleon. With increasing angular momentum up to $J \sim 30$, the yield of carbon increases faster than the yield of calcium, and at larger angular momenta the opposite trend is observed. The reason is that the difference in the potential energies of the DNS with a carbon nucleus and the DNS with a calcium nucleus decreases with increasing J (see Fig. 1) because of the difference in the moments of inertia of these configurations. So, the angular momentum strongly influences the probability of complex fragment emission.

The calculated A distributions and the isotopic distribution of the emitted products are shown in Fig. 6 (lower) and Fig. 8 for the reaction ^{78}Kr + ^{12}C at the bombarding energies E_{lab} = 8.52 and 11.37 MeV/nucleon. One can see that at higher energies the isotopic distributions of the light products become broader, but the positions of maxima remain almost the same.

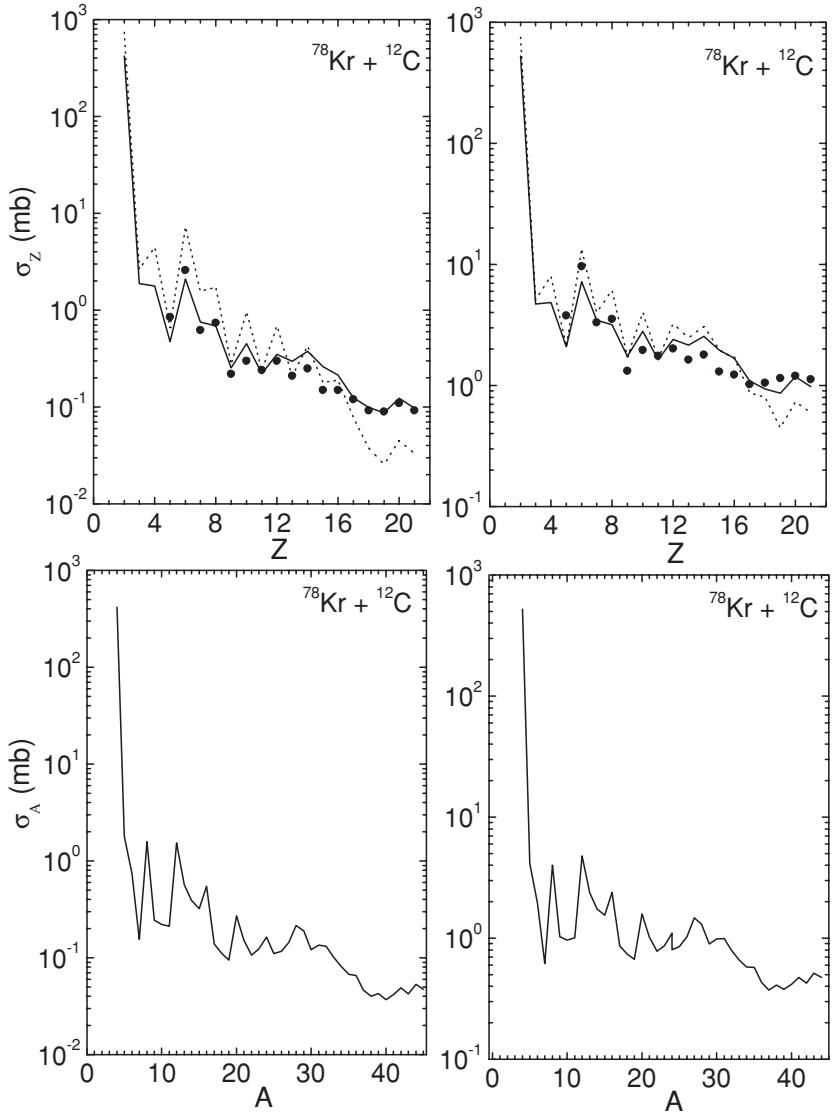

FIG. 6. Calculated charge (upper) and mass (lower) distributions for the ^{78}Kr + ^{12}C reaction at bombarding energies $E_{\rm lab} = 8.52$ MeV/nucleon (left) and 11.37 MeV/nucleon (right). Experimental data (filled points) are taken from Ref. [17]. Charge distributions calculated with Eq. (23) are shown by the dashed line.

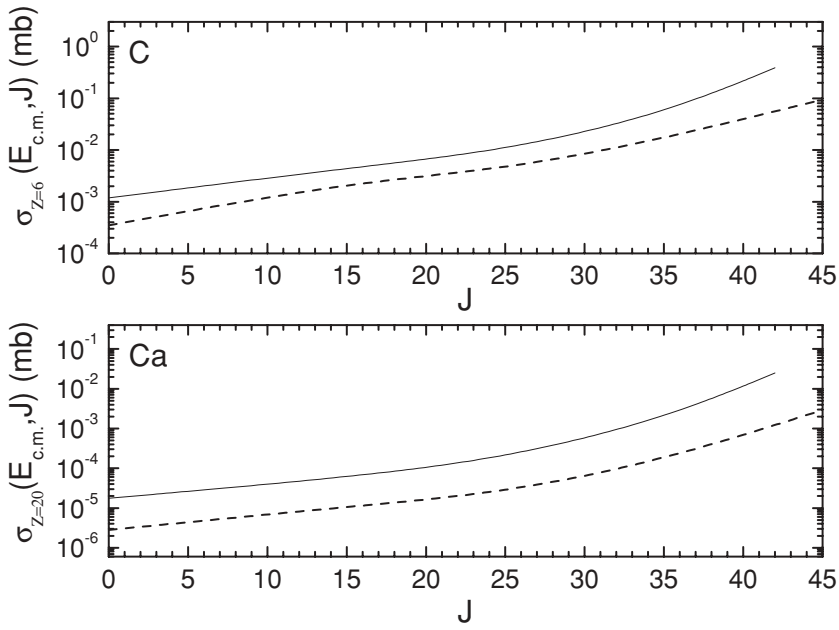

FIG. 7. Dependencies of the partial emission cross sections of carbon and calcium fragments on the angular momentum for the reactions ^{78}Kr ($E_{\rm lab} = 8.52$ MeV/nucleon) + ^{12}C (dashed lines) and ^{86}Kr ($E_{\rm lab} = 9.31$ MeV/nucleon) + ^{12}C (solid lines).

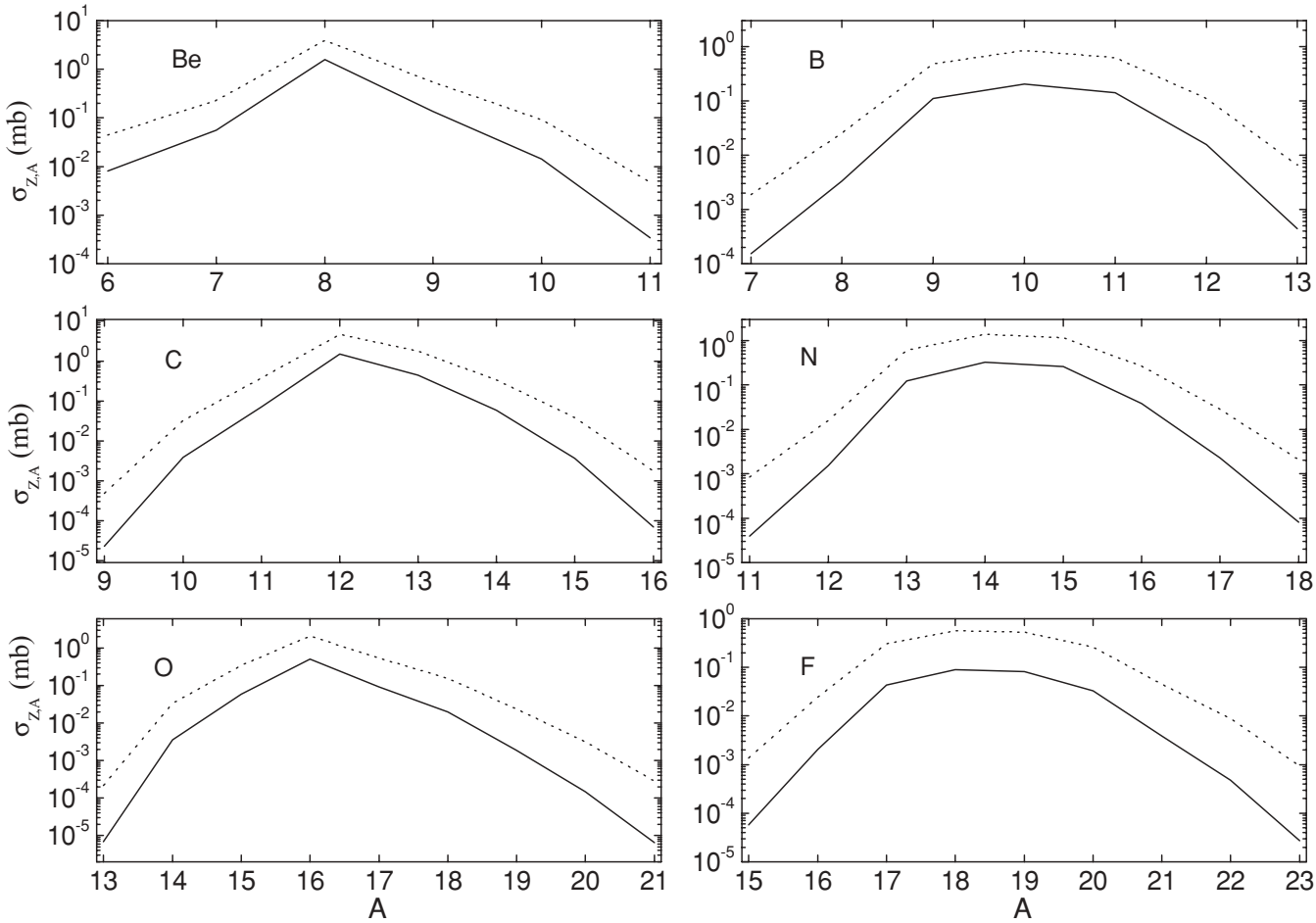

FIG. 8. Calculated isotopic distributions of binary decay products for the ^{78}Kr + ^{12}C reaction at bombarding energies $E_{\rm lab}$ = 8.52 MeV/nucleon (solid line) and 11.37 MeV/nucleon (dotted line).

The dependence of the average total kinetic energy,

$$\mathrm{TKE}(Z) = \sum_{A,J=0}^{J_{\max}} \left[U(R_b, Z, A, J=0) + \frac{\hbar^2 f J(fJ+1)}{2\mu R_b^2} \right] \frac{\sigma_{Z,A}(E_{\rm c.m.}, J)}{\sigma_Z(E_{\rm c.m.})}, \qquad f = \frac{0.85\mu R_m^2}{\Im(R_m, A, \beta_1, \beta_2)}, \tag{20}$$

of the binary decay products versus the charge asymmetry is predicted in Fig. 9 for the ^{78}Kr + ^{12}C reaction at $E_{\rm lab}$ = 8.52 MeV/nucleon. The average TKE follows the value of the corresponding Coulomb barrier and grows globally with increasing $Z \times Z_2$. So, the maximum of TKE at near-symmetry reflects the trend of the Coulomb interaction between one fragment and its partner.

The calculated charge and mass distributions of the binary decay products for the ^{86}Kr + ^{12}C reaction at $E_{\rm lab}$ = 9.31 and 12.94 MeV/nucleon are presented in Fig. 10. There, $J_{\max} = J_{\rm cr} = 45$ and $E^*_{\rm CN}(J=0) = 102.9$ and 141.1 MeV for the CN ^{98}Mo. Our method allows us to make a quantitative prediction of the charge distribution with the odd-even staggering structure. At higher excitation energies, the CN decays again, with a high probability by complex fragment emission. Comparing the results for the ^{78}Kr + ^{12}C and ^{86}Kr + ^{12}C

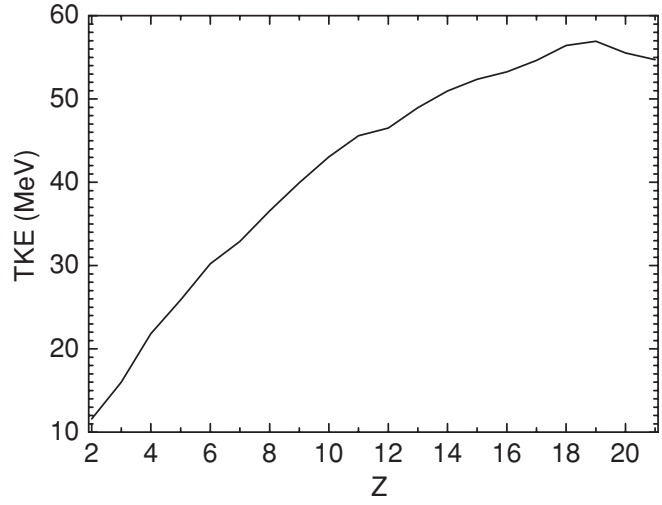

FIG. 9. Average total kinetic energy of fragments for the ^{78}Kr + ^{12}C reaction at bombarding energy $E_{\rm lab}$ = 8.52 MeV/nucleon.

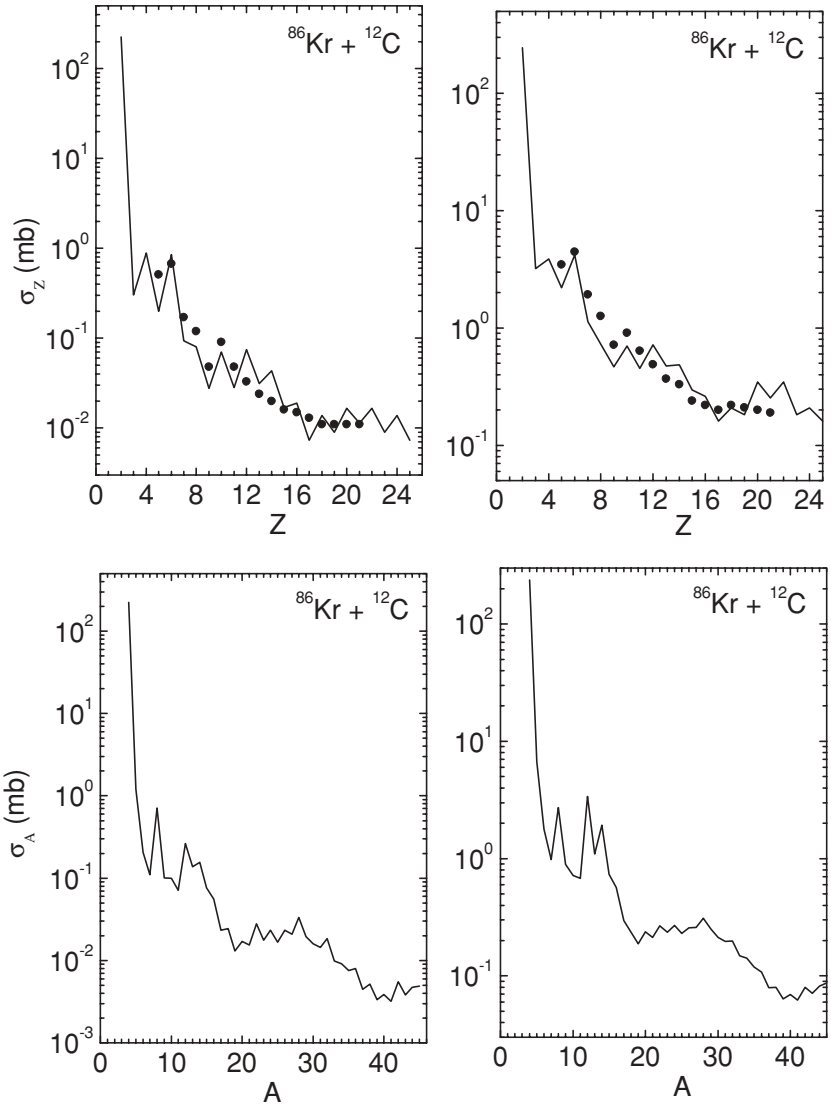

FIG. 10. Calculated charge (upper) and mass (lower) distributions for the ^{86}Kr + ^{12}C reaction at bombarding energies $E_{\rm lab} = 9.31$ MeV/nucleon (left) and 12.94 MeV/nucleon (right).

reactions leading to the CNs ^{90}Mo and ^{98}Mo, respectively, in Figs. 6 and 10, one can conclude that the emission cross sections for clusters with large Z are larger for the neutron-deficient CN. For instance, for carbon production, the ratio of the cross sections is 2.5. This can be explained by suppression of neutron evaporation from the neutron-deficient CN and by smaller mass-asymmetric fission barriers $U(R_b, Z, A, J)$ for the CN ^{90}Mo in comparison to the CN ^{98}Mo (see Fig. 2).

For the reactions ^{78}Kr + ^{12}C at $E_{\rm lab} = 8.52$ MeV/nucleon and ^{86}Kr + ^{12}C at $E_{\rm lab} = 9.31$ MeV/nucleon, the average excitation energy,

$$E^*_L(Z) = \sum_{A,J=0}^{J_{\max}} E^*_L(Z, A, J)\sigma_{Z,A}(E_{\rm c.m.}, J)/\sigma_Z(E_{\rm c.m.}), \quad (21)$$

and the average collective spin

$$J_L(Z) = \sum_{A,J=0}^{J_{\max}} J_L(Z, A, J)\sigma_{Z,A}(E_{\rm c.m.}, J)/\sigma_Z(E_{\rm c.m.}),$$
$$J_L(Z, A, J) = \frac{0.85\Im_1 J}{\Im(R_m, A, \beta_1, \beta_2)}, \quad (22)$$

of the primary light products as functions of Z are presented in Fig. 11. The results of calculations show that for light nuclei with $Z \lesssim 10$, the excitation energy is below the neutron emission threshold, and these nuclei do not decay further. For symmetric decay, the decay products have an excitation energy and spin of about of 20 MeV and 5, respectively, which are high enough for the emission of a few light particles.

In our method the emission of a given cluster from an excited CN is treated as a two-step process. If emission is assumed to be a one-step process—that is, the system directly overcomes the Coulomb barrier $U(R_b, Z, A, J)$ and emits fragments—the cross section of the charge particle emission is expressed as follows:

$$\sigma_{Z,A}(E_{\rm c.m.}) = \sum_{J=0}^{J_{\max}} \sigma_{\rm cap}(E_{\rm c.m.}, J) \times \frac{\exp[-U(R_b, Z, A, J)/T_{\rm CN}(J)]}{\sum_{Z',A'} \exp[-U(R_b, Z', A', J)/T_{\rm CN}(J)]}, \quad (23)$$

where the emission probability $W_{Z,A}(E^*_{\rm CN}, J)$ of a given cluster from the excited system is

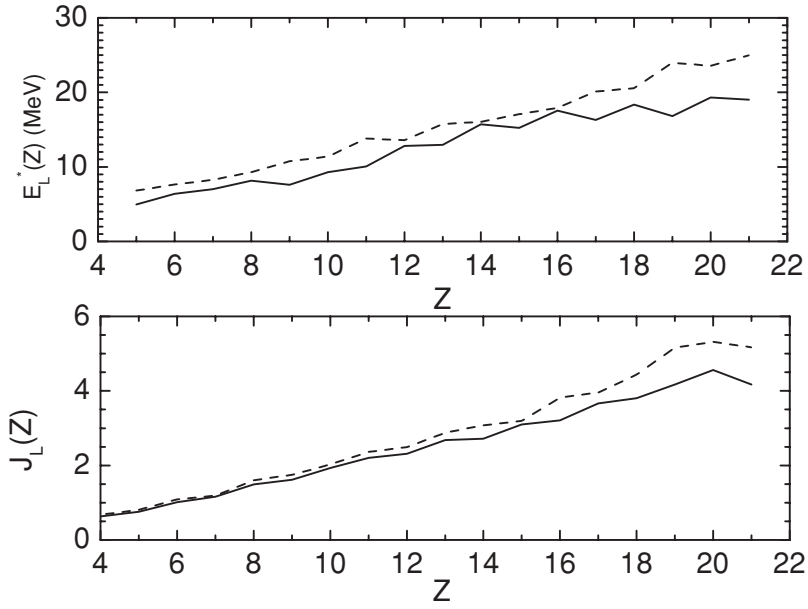

FIG. 11. Average excitation energies (upper) and spins (lower) of primary decay products for the reactions ^{78}Kr ($E_{\rm lab} = 8.52$ MeV/nucleon) + ^{12}C (solid lines) and ^{86}Kr ($E_{\rm lab} = 9.31$ MeV/nucleon) + ^{12}C (dashed lines).

$$W_{Z,A}(E^*_{\rm CN}, J) = \frac{\exp[-U(R_b, Z, A, J)/T_{\rm CN}(J)]}{\sum_{Z',A'} \exp[-U(R_b, Z', A', J)/T_{\rm CN}(J)]} = \frac{\exp\left[-\left[U(R_m, Z, A, J) + B^{qf}_R(Z, A, J)\right]/T_{\rm CN}(J)\right]}{\sum_{Z',A'} \exp\left[-\left[U(R_m, Z', A', J) + B^{qf}_R(Z', A', J)\right]/T_{\rm CN}(J)\right]}. \quad (24)$$

In Fig. 6 we compare the emission cross sections calculated by formulas (15) and (24). The difference between the results of these two methods decreases with increasing excitation energy of the CN. One can see that the two-step process treatment seems to be more suitable than the one-step process treatment. This fact supports the mechanism of cluster emission suggested by us. By using different level density parameters for the binary decay and evaporation of neutrons, one can obtain, with Eq. (24), better agreement with the experimental data.

IV. SUMMARY

The formalism developed in this paper allows us to describe the emission of a sizable fragment. The mechanism of cluster emission is treated under the assumption that light clusters are produced by a collective motion of the nuclear system in the charge asymmetry coordinate, with further thermal penetration through the Coulomb barrier. The emission barriers for complex fragments are calculated by using the double-folding formalism for the nuclear part of the nucleus-nucleus interaction potential. Competition between the evaporation channel and the binary decay channel is taken into consideration in a unique way. This competition and the competition between the binary decay channels strongly depend on the angular momentum of the system.

Our approach describes the experimental production cross sections for complex fragments well . Therefore, one can expect that the suggested treatment will provide reasonable estimates of mass distributions of nuclear decays by cluster emissions. The predicted dependence of the cross section of binary decay on the isotopic composition of the CN correlates well with the isotopic dependence of the Q value. The theoretical predictions of the isotopic distributions for the reactions ^{3}He + $^{\rm nat}$Ag and ^{78}Kr + ^{12}C can be experimentally checked by measuring the cross sections of the emission of different sizable clusters as functions of the excitation energy. Irregularities in the increase in emission of various clusters with excitation energy would reflect certain charge and mass asymmetric states. The optimal excitation energies for emission of different complex fragments and the TKE distribution of binary decay products can also be predicted with our model.

ACKNOWLEDGMENTS

We thank Drs. D. Lacroix, V. V. Sargsyan and J.-P. Wieleczko for the useful discussions and suggestions. This work was supported by the DFG and RFBR. The IN2P3-JINR, MTA-JINR, and Polish-JINR Cooperation programs are gratefully acknowledged.

[1] W. G. Lynch, Annu. Rev. Nucl. Sci. **37**, 493 (1987).
[2] L. G. Moretto and G. J. Wozniak, Prog. Part. Nucl. Phys. **21**, 401 (1988).
[3] J. Töke, J. Lu, and W.-U. Schröder, Phys. Rev. C **67**, 034609 (2003); B. Djerroud *et al.*, *ibid.* **64**, 034603 (2001); J. Töke, D. K. Agnihotri, W. Skulski, and W.-U. Schröder, *ibid.* **63**, 024604 (2001).
[4] E. Bonnet *et al.*, Int. J. Mod. Phys. E **17**, 2359 (2008); J.-P. Wieleczko *et al.*, Acta Phys. Pol. B **40**, 577 (2009); in *Proceedings, International Conference on Nuclear Structure and Related Topics* (JINR, Dubna, 2009), p. 236.
[5] U. Lynen *et al.*, Nucl. Phys. A **387**, 129 (1982).
[6] C. B. Chitwood *et al.*, Phys. Lett. B **131**, 289 (1983).
[7] B. V. Jacak *et al.*, Phys. Rev. Lett. **51**, 1846 (1983).
[8] L. G. Sobotka *et al.*, Phys. Rev. Lett. **51**, 2187 (1983).
[9] L. G. Sobotka *et al.*, Phys. Rev. Lett. **53**, 2004 (1984).
[10] M. A. McMahan, L. G. Moretto, M. L. Padgett, G. J. Wozniak, L. G. Sobotka, and M. G. Mustafa, Phys. Rev. Lett. **54**, 1995 (1985).
[11] R. Vandenbosch and J. R. Huizenga, *Nuclear Fission* (Academic Press, New York, 1973).
[12] L. G. Moretto, Nucl. Phys. A **247**, 211 (1975).
[13] W. A. Friedman and W. G. Lynch, Phys. Rev. C **28**, 16 (1983).
[14] A. J. Cole, *Statistical Models for Nuclear Decay* (Institute of Physics, London, 2000).
[15] R. J. Charity *et al.*, Nucl. Phys. A **483**, 371 (1988); **476**, 516 (1988).
[16] A. J. Sierk, Phys. Rev. Lett. **55**, 582 (1985).
[17] K. X. Jing *et al.*, Nucl. Phys. A **645**, 203 (1999).
[18] J. Boger and J. M. Alexander, Phys. Rev. C **50**, 1006 (1994).
[19] V. V. Volkov, Izv. Akad. Nauk SSSR, Ser. Fiz. **50**, 1879 (1986); G. G. Adamian, N. V. Antonenko, and W. Scheid, Nucl. Phys. A **618**, 176 1997; G. G. Adamian, N. V. Antonenko, W. Scheid, and V. V. Volkov, *ibid.* **627**, 361 (1997); **633**, 409 (1998).
[20] A. S. Zubov, G. G. Adamian, N. V. Antonenko, S. P. Ivanova, and W. Scheid, Phys. Rev. C **68**, 014616 (2003).
[21] G. G. Adamian, N. V. Antonenko, R. V. Jolos, S. P. Ivanova, and O. I. Melnikova, Int. J. Mod. Phys. E **5**, 191 (1996).
[22] G. G. Adamian, N. V. Antonenko, and W. Scheid, Nucl. Phys. A **678**, 24 (2000).
[23] S. Raman Jr., C. W. Nestor, and P. Tikkanen, At. Data Nucl. Data Tables **78**, 1 (2001).
[24] G. Audi, A. M. Wapstra, and C. Thibault, Nucl. Phys. A **729**, 337 (2003).
[25] P. Möller *et al.*, At. Data Nucl. Data Tables **59**, 185 (1995).
[26] S. Åberg and L.-O. Jönsonn, Annu. Rev. Nucl. Part. Sci. **40**, 439 (1990); S. Åberg, Nucl. Phys. A **557**, 17 (1993); Z. Phys. A **349**, 205 (1994).
[27] A. B. Migdal, *Theory of Finite Fermi Systems and Properties of Atomic Nuclei* (Nauka, Moscow, 1983).
[28] A. V. Ignatyuk, *Statistical Properties of Excited Atomic Nuclei* (Energoizdat, Moscow, 1983).
[29] G. G. Adamian, A. K. Nasirov, N. V. Antonenko, and R. V. Jolos, Phys. Part. Nuclei **25**, 583 (1994); G. G. Adamian, N. V. Antonenko, R. V. Jolos, and A. K. Nasirov, Nucl. Phys. A **551**, 321 (1993).
[30] H. Y. Han *et al.*, Nucl. Phys. A **492**, 138 (1989).
[31] R. Bass, Phys. Rev. Lett. **39**, 265 (1977).